In situ conductivity characterization of oxide thin film growth phenomena on microhotplates

F. DiMeo, R. E. Cavicchi, S. Semancik, J. S. Suehle, N. H. Tea et al.

Citation: J. Vac. Sci. Technol. A 16, 131 (1998); doi: 10.1116/1.580959
View online: http://dx.doi.org/10.1116/1.580959
View Table of Contents: http://avspublications.org/resource/1/JVTAD6/v16/i1
Published by the AVS: Science & Technology of Materials, Interfaces, and Processing

Related Articles

X-ray photoelectron spectroscopic study on interface bonding between Pt and Zn- and O-terminated ZnO
J. Vac. Sci. Technol. A 31, 020601 (2013)

Atomic layer deposition of zinc sulfide with Zn(TMHD)2
J. Vac. Sci. Technol. A 31, 01A138 (2013)

New approach toward transparent and conductive ZnO by atomic layer deposition: Hydrogen plasma doping
J. Vac. Sci. Technol. A 31, 01A130 (2013)

Mixed Magnesium and Zinc Oxide Prepared by Co-precipitation and Analyzed by XPS
Surf. Sci. Spectra 19, 13 (2012)

Band alignment of zinc oxide as a channel layer in a gate stack structure grown by plasma enhanced atomic layer deposition
J. Vac. Sci. Technol. B 30, 051807 (2012)

Additional information on J. Vac. Sci. Technol. A

Journal Homepage: http://avspublications.org/jvsta
Journal Information: http://avspublications.org/jvsta/about/about_the_journal
Top downloads: http://avspublications.org/jvsta/top_20_most_downloaded
Information for Authors: http://avspublications.org/jvsta/authors/information_for_contributors

ADVERTISEMENT

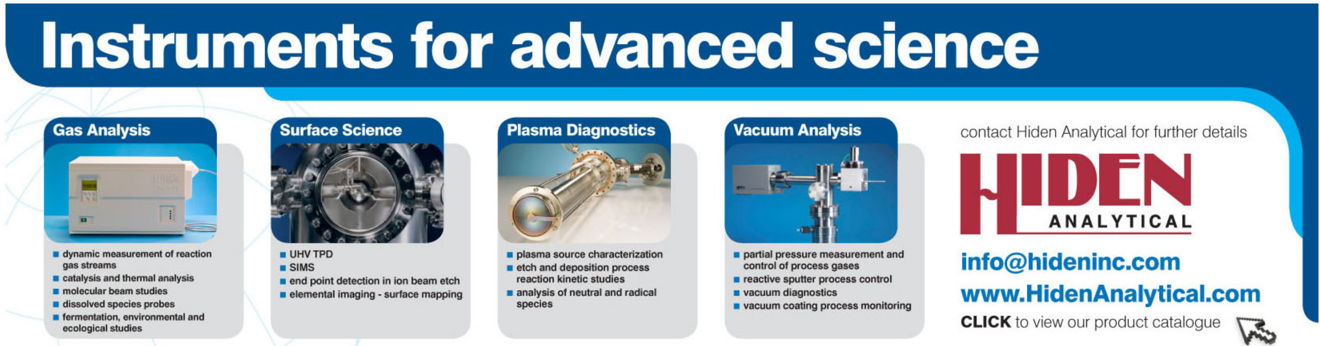

Downloaded 14 Jan 2013 to 202.38.84.14. Redistribution subject to AVS license or copyright; see http://avspublications.org/jvsta/about/rights_and_permissions

In situ conductivity characterization of oxide thin film growth phenomena on microhotplates

F. DiMeo, Jr.,[a] R. E. Cavicchi, and S. Semancik[b]
Process Measurements Division, National Institute of Standards and Technology, Gaithersburg, Maryland 20899

J. S. Suehle and N. H. Tea
Semiconductor Electronics Division, National Institute of Standards and Technology, Gaithersburg, Maryland 20899

J. Small and J. T. Armstrong
Surface and Microanalysis Science Division, National Institute of Standards and Technology, Gaithersburg, Maryland 20899

J. T. Kelliher
Microelectronics Research Laboratory, Columbia, Maryland 21045

(Received 14 April 1997; accepted 30 October 1997)

Through the use of silicon micromachining, we have developed a microhotplate structure capable of reaching temperatures in excess of 500 °C, onto which thin films have been selectively grown via metalorganic chemical vapor deposition. The microhotplate structure contains surface electrical contacts which permit conductance measurements to be made on films during and after deposition, and therefore presents some unique opportunities for the *in situ* characterization of growing films as well as for novel gas sensing approaches. We have investigated the deposition of conducting oxides such as SnO_2 and ZnO on these microhotplate platforms for gas sensing applications. The conductance of the deposited films has been measured *in situ* as a function of time, and used in combination with postdeposition thickness measurements to provide insights into the growth rate of the oxide films. Results indicate that our conductance measurements are sensitive, in certain cases, to changes in the film thickness on the order of an angstrom. Conductance oscillations observed during the growth of ZnO thin films have been attributed to variations in the precursor concentration, and were detected as a gas sensor response by the growing films. © *1998 American Vacuum Society.* [S0734-2101(98)03701-4]

I. INTRODUCTION

Conductometric gas sensors using semiconducting oxides as the active material have been used to detect a variety of gaseous species.[1] In particular, SnO_2 and ZnO have been extensively studied, and have been used as the base material in devices such as the Taguchi sensor[2] and the ZnO varistor.[3] Such discrete devices, however, can be application limited by their lack of specificity, long term drift behavior, relatively high power consumption, and cost. To advance past these difficulties, we have been developing arrays of thin film conductometric gas sensors using planar silicon micromachining techniques. Currently, the arrays consist of four microhotplate elements, each having a suspended polysilicon resistive heater with a thermal rise time of $\sim$3 ms, and maximum operating temperature of 550 °C. Since the adsorption/desorption phenomena critical to the sensing process are temperature dependent, these suspended structures contain a thin film thermometer and heat distribution plate for improved thermal control. There are also four contact pads on the surface of the microhotplate for measuring the conductance of the active film.[4]

[a]Present address: Advanced Technology Materials, Inc., Danbury, CT 06810; Electronic mail: fdimeo@atmi.com
[b]Electronic mail: steves@nist.gov

The contact pads serve a dual purpose. They are used to measure the change in conductance of the active layer when it is exposed to various gases as a sensor, but they also present a unique opportunity for the *in situ* conductance measurements of growing thin films.[5] This monitoring technique is particularly useful when studying the metalorganic chemical vapor deposition (MOCVD) process for oxides, where other *in situ* characterization techniques such as reflection high-energy electron diffraction (RHEED), or low-energy electron diffraction (LEED) are unavailable because of the high background pressures involved. We have chosen the MOCVD process for film fabrication because it provides an extremely efficient way to deposit varied types of active layers on arrays of microhotplate devices. The thermally activated nature of our MOCVD processing results in self-lithographic, selected area deposition that minimizes the number of processing steps required to fabricate multiple material layers within a given array.

In this article we will present recent *in situ* conductance measurements of SnO_2 and ZnO thin films as they were deposited onto microhotplates, and explore the characterization capabilities possible with this real-time monitoring technique.

Downloaded 14 Jan 2013 to 202.38.84.14. Redistribution subject to AVS license or copyright; see http://avspublications.org/jvsta/about/rights_and_permissions

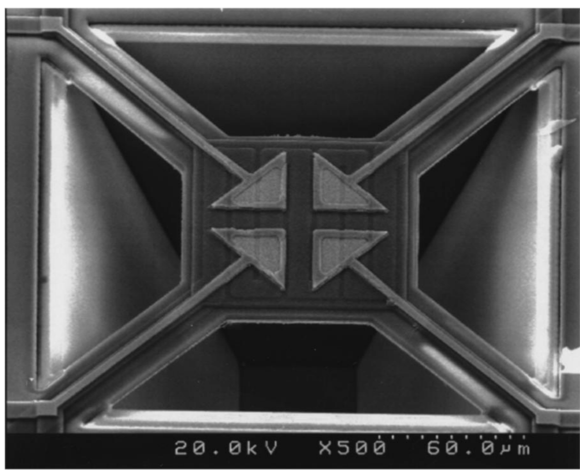

FIG. 1. SEM image of a single microhotplate structure after exposure to EDP etchant solution. The image was taken at a tilt angle of 35°.

II. EXPERIMENT

In this work, SnO_2 and ZnO thin films were deposited on microhotplate arrays using MOCVD. There were two basic designs of microhotplates, those fabricated through the Metal Oxide Semiconductor Implementation Service (MOSIS), and those fabricated using a tungsten metallization process at the Microelectronics Research Laboratory (MRL). The fabrication of the microhotplate arrays through MOSIS is described in detail elsewhere,[4,6] and is briefly as follows. The chips were designed using the software package MAGIC, and sent through the MOSIS foundry process. This process is based on a standard complementary metal–oxide–semiconductor (CMOS) fabrication line with a 2.0 μm feature size and uses aluminum as the metallization material in two levels. Devices fabricated at MRL were based on a design similar to that fabricated through MOSIS, with the exception that tungsten, instead of aluminum, was used for both levels of metallization. The chips from MOSIS were etched using XeF_2 to preferentially, but isotropically, remove the exposed single crystal silicon and form the suspended microbridge. Sputtered Cr/Ir metal layers were used to coat the Al contacts. Chips received from MRL were etched in ethylenediamminepyrocatechol (EDP) and water solution to preferentially and anisotropically remove the exposed silicon to produce the suspended microbridge structure. Figure 1 shows a single MRL fabricated microhotplate device (at a viewing angle of 35°) after etching in EDP. In contrast to the aluminum present in MOSIS devices, the tungsten was not attacked by the EDP solution, which is a significant advantage, since no additional steps were needed to protect the contact areas. In both the MOSIS and MRL cases, the etched die were mounted in 40 pin dual-in-line chip packages, and wirebonded with aluminum leads.

The MOCVD system used for thin film deposition is schematically illustrated in Fig. 2. Tetramethyltin (TMT) (99.999% pure from Morton Advanced Chemicals[7]) and diethylzinc (DEZ) (99.999% pure from Akzo Nobel[7]) were used as the metal sources. Ultrahigh purity argon (99.9995%) was used as the carrier gas, and the reactant gas was oxygen (99.995%).

Packaged chips were placed in a socket inside the reactor and electrical connections to the socket were made through a 40 pin vacuum feedthrough. The microsubstrate temperatures were determined at each operating pressure from the calibrated change in resistance of the polysilicon heater resistance. These agreed to within $\sim$5% of the temperatures determined in a similar manner from the change in aluminum metal plate resistance values. Control of the microhotplates was established in two different ways, a manual mode and a computer automated mode. In the manual mode, heating currents to the microhotplates were supplied individually by a Keithley 220 current source.[7] A separate current source was used in conjunction with a Keithley 2001 storage multimeter[7] to make resistance measurements on the films during and after deposition. Up to 6000 readings taken at intervals of 0.002–2 s could be logged during one run. This acquisition capability allowed the observation of transient phenomenon during growth, and provided increased thickness resolution of the technique. Automated computer con-

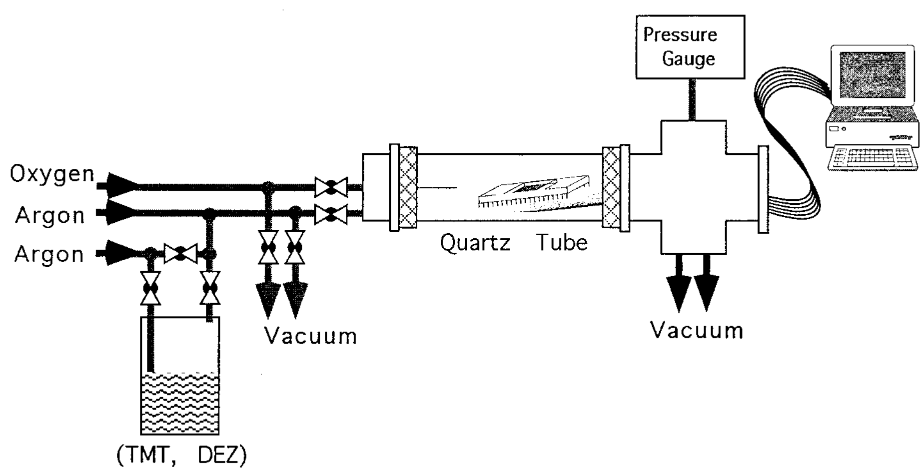

FIG. 2. Schematic diagram of the MOCVD deposition system.

Downloaded 14 Jan 2013 to 202.38.84.14. Redistribution subject to AVS license or copyright; see http://avspublications.org/jvsta/about/rights_and_permissions

TABLE I. Typical growth conditions for films deposited on microhotplates.

	Tetramethlytin (TMT)	Diethylzinc (DEZ)
Precursor temperature	−40 to −50 °C	−30 to −15 °C
Vapor pressure	203–414 Pa	53–171 Pa
Total pressure	0.130–101 kPa (1–760 Torr)	0.130–1.3 kPa (1–10 Torr)
Microhotplate deposition temperature	350–550 °C	350–550 °C
Microhotplate heater power	30–60 mW	30–60 mW
Total argon flow rate	200–500 sccm	200–500 sccm
Oxygen flow rate	200–600 sccm	100–300 sccm

trol of the system was achieved by using a four-channel digital/analog (D/A) card to supply current to the heaters, and a switching box to measure the conductivity of the surface films sequentially. Either the growth time or the resistance of the growing thin film could be used as feedback to terminate the deposition by turning off the heater power. Typical growth conditions are summarized in Table I.

III. RESULTS AND DISCUSSION

We have reported previously on thin film growth via MOCVD of SnO_2 and ZnO on microhotplates;[4,5,8–11] in this work the usefulness of *in situ* conductance measurements was explored. In Sec. III A, *in situ* conductance data taken over the course of the entire film deposition will be presented, and four different growth regions (I–IV) will be discussed. Section III B discusses the use of measurements of the width of region I as a means of improving process control. In Sec. III C, thickness measurements will be coupled with the *in situ* conductivity data from region III in order to determine the effect of variations in the precursor composition on the growth rate and to probe the ultimate thickness sensitivity of these measurements. Finally, in Sec. III D an example will be given that demonstrates the usefulness of these measurements as an *in situ* process diagnostic tool.

A. *In situ* conductance monitoring

Figure 3 shows linear and semilog plots of representative electrical conductance data taken during the deposition of SnO_2 [Fig. 3(A)] and ZnO [Fig. 3(B)] on a MOSIS chip. In each case, the curves can be divided into four regions. There is an initial plateau labeled region I, followed by an increasing but nonlinear behavior labeled region II. Then the films exhibit a linear behavior labeled region III, and finally there is a sharp drop in conductance, labeled region IV, which occurs when the power to the heater is turned off and growth stops. *In situ* conductance measurements taken during the growth of thin films on MRL chips are qualitatively the same, but exhibit time scales that are longer by as much as a factor of 5 and larger grain sizes. This slower deposition rate is attributed to differences in the thin film nucleation rate that result from variations in the top SiO_2 layers due to the different silicon etching processes. Figure 4 shows a series of three scanning electron microscopy (SEM) images to illustrate the morphology of different regions (I–III) in the con-

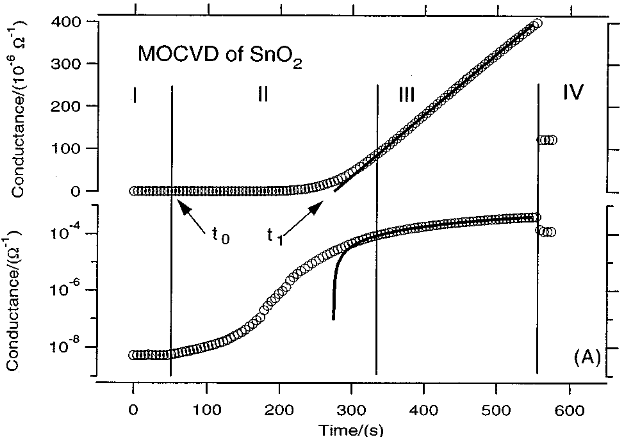

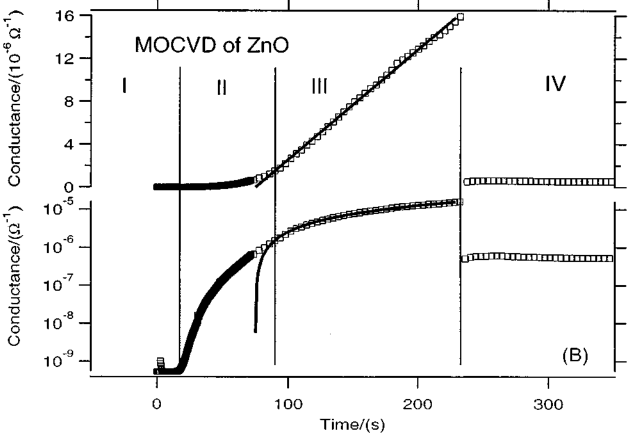

FIG. 3. *In situ* conductance vs time data for the growth of (A) a SnO_2 film and (B) a ZnO film on MOSIS hotplate structures within the same array. The SnO_2 film was deposited under the following conditions: hotplate temperature=475 °C, TMT temperature=−45 °C with 8 sccm of carrier gas flow, a total pressure of 0.77 kPa, and a partial pressure of oxygen of 0.37 kPa. The conditions for the ZnO film deposition were hotplate temperature of 400 °C, a DEZ temperature=−19 °C and no carrier gas flow, a total pressure of 0.60 kPa, and a partial pressure of oxygen of 0.21 kPa. Both linear and semilog plots are shown. The four marked regions separate different stages of growth. Region I is the early phase of the film growth where the material has not yet formed a continuous layer. Region II is the region of loosely connected film, where there is an increasing number of conduction paths and a measurable conductance. Region III is the linear growth region, where there is a uniformly covered substrate and a constant deposition of material. The solid lines are the linear fit to the data in region III. Region IV is the room temperature conductance of the fully connected film, after the growth has been terminated.

Downloaded 14 Jan 2013 to 202.38.84.14. Redistribution subject to AVS license or copyright; see http://avspublications.org/jvsta/about/rights_and_permissions

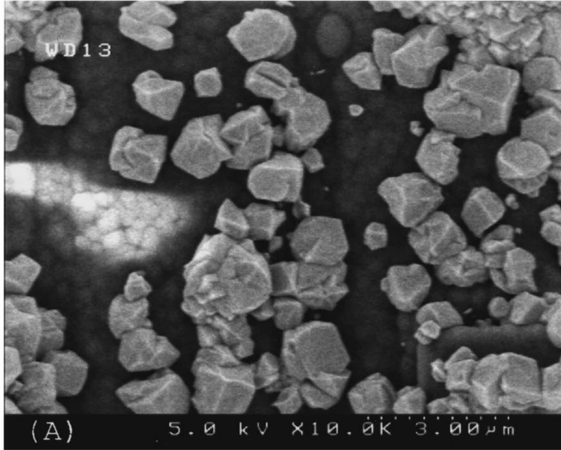

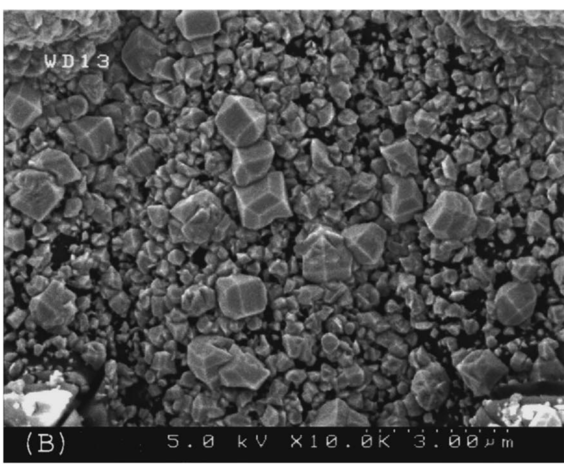

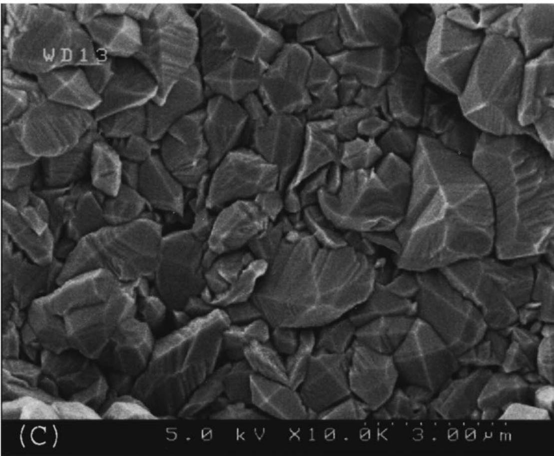

FIG. 4. SEM images of SnO_2 thin films deposited on MRL hotplate structures that are representative of regions I–III in Fig. 3. The growth conditions for these films were a hotplate temperature of 475 °C, a TMT temperature of −48 °C with 8 sccm of carrier gas flow, a total pressure of 0.76 kPa, and a partial pressure of oxygen of 0.35 kPa, and times of 310, 510, and 950 s for (A), (B), and (C), respectively. (A) Grains are dispersed and mostly unconnected. (B) The density of grains has increased, but the substrate is still discernible through gaps in the film. (C) The film is fully connected across the microhotplate.

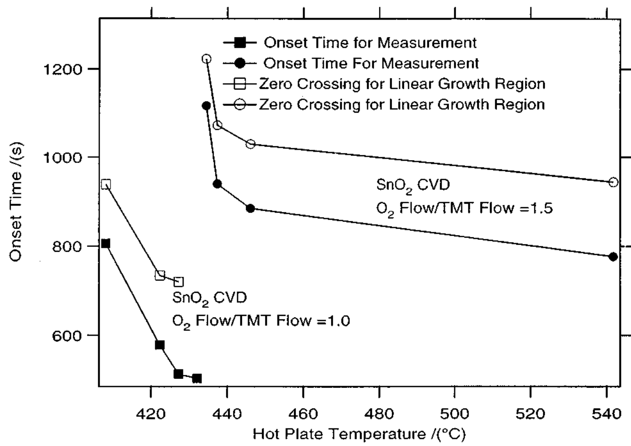

FIG. 5. SnO_2 thin film growth onset time vs microhotplate temperature. The determination of the onset time is described in the text.

ductance data. These images are of three SnO_2 films grown on MRL devices within the same array under identical conditions, but stopped at different times. The slower growth rate of films deposited on MRL chips results in large faceted grains, and is more easily interrupted in a particular region than films grown on MOSIS chips. In Fig. 4(A) we see generally unconnected grains, whereas in Fig. 4(B) the grains are starting to join into a connected network, and finally in Fig. 4(C), the film is dense and completely continuous. Also visible in Fig. 4(A) is the morphology of the underlying SiO_2 layer between grains, which gradually disappears as the SnO_2 coverage increases. In combination with the electrical behavior seen on both MOSIS and MRL chips, the micrographs suggest that region I is the early phase of the film growth. In this phase, material is beginning to nucleate and deposit on the substrate but has not formed a continuous layer, and so does not lead to a measurable conductance increase. Region II is a region of loosely connected film, where there is an increasing number of conduction paths and a measurable conductance. This exhibits nonlinear behavior because of the increasing number of conducting paths that form and increase in size as new connections between grains are made. Region III is the linear growth region, where there is a uniformly covered substrate and a constant deposition of material resulting in a steady increase of conductance with time. The solid lines in Figs. 3(A) and 3(B) are the linear fits to the data in region III. Finally, region IV is the room temperature conductance of the fully connected film, after the growth has been terminated by shutting off the power to the heater. The drop in conductance is due to the loss of thermally activated carriers.

B. *In situ* measurements for improved process control

Process reproducibility is an important concern if these devices are to be used successfully as gas sensors. Figure 5 shows the behavior of onset time of film growth versus growth temperature for two four-element arrays grown under different ratios of oxygen/TMT. The open symbols show the

Downloaded 14 Jan 2013 to 202.38.84.14. Redistribution subject to AVS license or copyright; see http://avspublications.org/jvsta/about/rights_and_permissions

onset time of measurable conductance, which is the duration of region I as in Fig. 3. The closed symbols are for the onset times that are taken as the zero thickness intercept of a linear fit to region III, i.e., t_1 from Fig. 3, the equivalent starting point if the film growth proceeded constantly and uniformly at all times. For both oxygen/TMT ratios, at low temperatures, the onset time increases dramatically with decreasing temperature. This is due to the temperature activation of both the nucleation rate and the conductivity at these low coverages. As the growth temperature increases, the sensitivity of the onset time to temperature decreases. Thus, from a processing point of view, depositing at a higher temperature results in a process that is faster and less sensitive to variation in temperature, and thus represents a better regime to work in, if other film properties are not compromised. The general decrease in onset time as a function of decreasing oxygen/TMT ratio is as expected because a higher tin content results in more conductive material, which will be detectable at smaller thicknesses. The unique capability to perform *in situ* conductance measurements has been used here both as a technique to study the growth and deposition of thin films and also as a tool to design a more robust deposition process.

C. Film thickness and *in situ* conductance measurements

To further analyze the *in situ* conductance data, it is instructive to look at the relationship between the measured conductance and the films' materials properties. In the following equation, the experimentally measured resistance, R, is expressed as the sum of the film resistance, $L/\sigma Wd$ and the contact resistance, R_c, where L and W are the length and width of the film between the contacts, d is the film thickness, and σ is the conductivity of the film.

$$R=\frac{L}{\sigma Wd}+R_c. \quad (1)$$

This equation assumes a homogeneous film, and thus can be applied only to region III, where the films are dense and continuous. The conductivity, σ, is a product of the number of carriers and their mobility, both of which will, in general, be dependent on temperature. The number of carriers will also be a function of the interactions of the solid with the ambient. The iridium or tungsten contact materials produce contact resistances that are small compared to the film resistances, so that, neglecting R_c, the conductance as a function of time, $S(t)$, is proportional to the conductivity and the thickness, as expressed by

$$S(t)=\sigma(t)\,\frac{Wd(t)}{L}. \quad (2)$$

Solution of Poisson's equation for the voltage distribution in two dimensions using finite element modeling of our device geometry indicates that this expression is valid when the distance between the contacts is much greater than the film thickness, i.e., for our geometry and film thicknesses, effects due to spreading resistance are negligible. The following is a case where we have been able to use this simple description of the conductivity to gain further insight into the film deposition process.

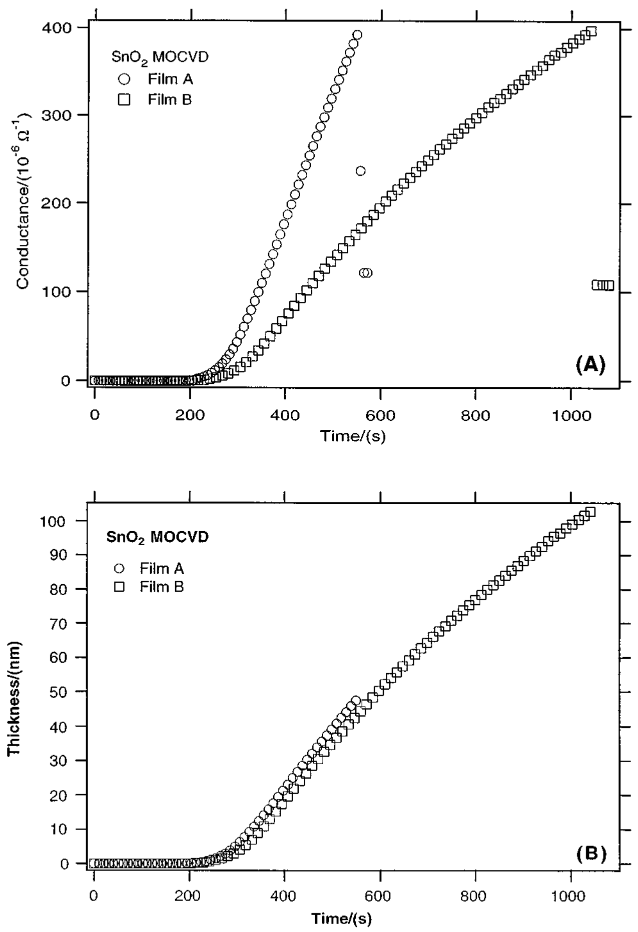

FIG. 6. (A) *In situ* conductance vs time data for the growth of two SnO_2 thin films. (B) Thickness vs time data derived from (A).

This example illustrates the deconvolution of growth rate from the conductance data. Two films (A and B) of SnO_2 were grown under identical conditions on MOSIS devices, with the exception that film B was grown with approximately 10% less TMT concentration than film A. This was achieved by changing the setpoint temperature of the TMT bath from −48 to −49 °C. Figure 6(A) is a plot of the *in situ* conductance versus time for these two films, and it can be seen that, even though the growth of both films was terminated at the same conductance value, the growth times were different by nearly 40%. Figure 7 shows these films have a similar morphology, with a grain size of ~30 nm. The uniformity of the morphology of these films suggests that they are more suitable candidates for the application of our simple model than the rougher highly faceted films produced on MRL devices seen in Fig. 4. The larger bubblelike features are due to the morphology of the underlying SiO_2 layer.

The question remains whether the change in TMT concentration changed the growth rate, the film conductivity, or some combination of the two. To answer this, independent measurements of the SnO_2 thickness on the microhotplate

Downloaded 14 Jan 2013 to 202.38.84.14. Redistribution subject to AVS license or copyright; see http://avspublications.org/jvsta/about/rights_and_permissions

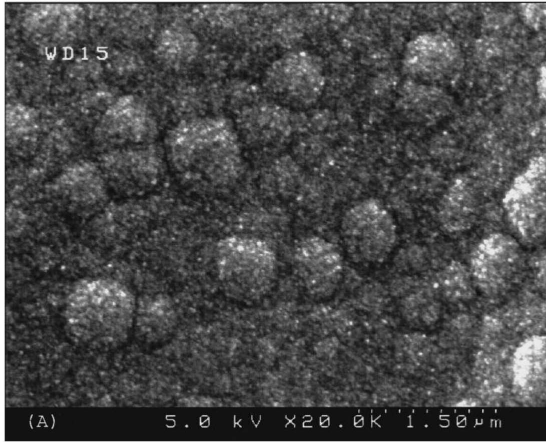

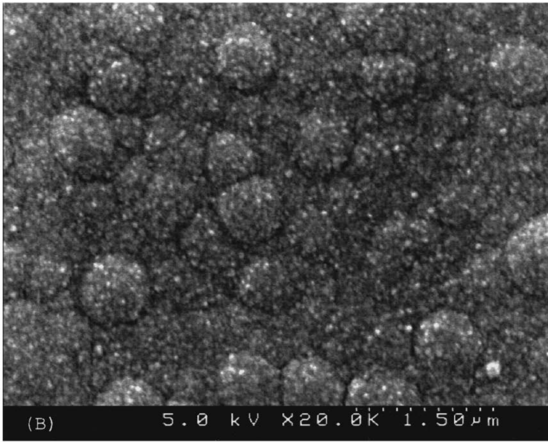

FIG. 7. SEM images of the SnO_2 films on MOSIS structures from Fig. 6. The morphologies of both (A) film A and (B) film B consist of small, dense grains ~30 nm in size. Larger, bubblelike features are due to conformal coating of the underlying substrate.

substrates are needed. Thickness measurements of deposited layers are difficult to make because of the small size and geometry of the microhotplate substrates. To overcome these challenges, we have used electron-probe x-ray microanalysis with wavelength dispersive spectrometry (WDS), in conjunction with film thickness modeling based on the algorithms of Pouchou and Pichoir.[12] For the purposes of this analysis, a stoichiometric composition of SnO_2 was assumed, and three different incident beam acceleration voltages (25, 15, and 8 keV) were used. Thicknesses of 48 ± 6 and 102 ± 9 nm were measured, respectively, for films A and B. Even though it is well known that oxygen vacancies are responsible for the conductivity in these materials, the assumption of stoichiometric composition is valid for this analysis because the vacancy concentrations, although electrically significant, are low enough so as not to alter the effective material density, which is the parameter of interest.

If the deposition process is at steady state, i.e., the deposition rate is constant; then a linear behavior in the conductance versus time data implies that the conductivity is constant in this region. In Fig. 6(A), film A displays a linearly

TABLE II. Values used to derive the thickness vs time behavior.

	Measured thickness (nm)	Final conductance ($\times10^{-4}\ \Omega^{-1}$)	$\frac{\text{Width}}{\text{length}}$	Final conductivity σ ($\Omega^{-1}\ \text{m}^{-1}$)
Film A	48 ± 6	4.009 ± 0.001	7.5	1100 ± 140
Film B	102 ± 9	4.002 ± 0.001	7.5	$520\pm\ 40$

increasing conductance with time at ~300 s into the growth and continues in this fashion until the growth is stopped ~260 s later. Film B also displays a linear behavior after ~300 s of growth, but begins to deviate slightly ~260 s later in the growth. This is most likely due to drift in either the microhotplate substrate temperature and/or the TMT vapor concentration due to variation in the bubbler bath temperature (~0.1 °C), which can cause slight changes in σ. For the purposes of this simple analysis however, both films will be treated in the constant conductivity limit. In this limit, with the fixed contact pad geometry and the final thickness measurements by WDS, values of σ (at the growth temperature) can be derived for each film and are listed in Table II. (The geometry in this case is based on connecting two adjacent pads together. The width to length ratio then becomes 75/10 μm or 7.5.) The conductance data can then be divided by this value of $\sigma W/L$ to yield thickness as a function of time, which is shown in Fig. 6(B). In Fig. 6, the growth rates for the two films are very similar, which indicates that the change in TMT concentration primarily affects the conductivity, and not the material deposition rate.

Further analysis of the growth rates of these films provides a measure of the thickness sensitivity of the *in situ* resistance technique. Figure 8(A) is a semilog plot of the thickness data, and shows that the linear behavior starts at an equivalent film thickness of ~8 nm. Figure 8(B) is an enlargement of the linear growth region, and shows that the change in equivalent thickness between measured points is less than 0.1 nm.

D. *In situ* CVD process gas sensor

This final example shows how the sensitivity of the conductance of ZnO films to their ambient growth conditions was used to detect variations in the precursor concentration during growth. Figure 9(A) shows the conductance versus time data for a growing ZnO film. These data were taken using a digital oscilloscope, and the breaks in the data occurred when the data were being downloaded to the computer. Overall, the expected increasing conductance with time behavior is observed, but the lower panel of Fig. 9(b) is an enlargement of one segment of the growth data, and reveals an oscillatory behavior. It is tempting to interpret this observation as a type of layer-by-layer growth phenomenon. This is unlikely for several reasons however. First, SEM analysis indicates that the films are polycrystalline and such a macroscale behavior would be unexpected from such a nonuniform surface. Second, a layer-by-layer process would be expected to result in a staircase conductivity behavior that

Downloaded 14 Jan 2013 to 202.38.84.14. Redistribution subject to AVS license or copyright; see http://avspublications.org/jvsta/about/rights_and_permissions

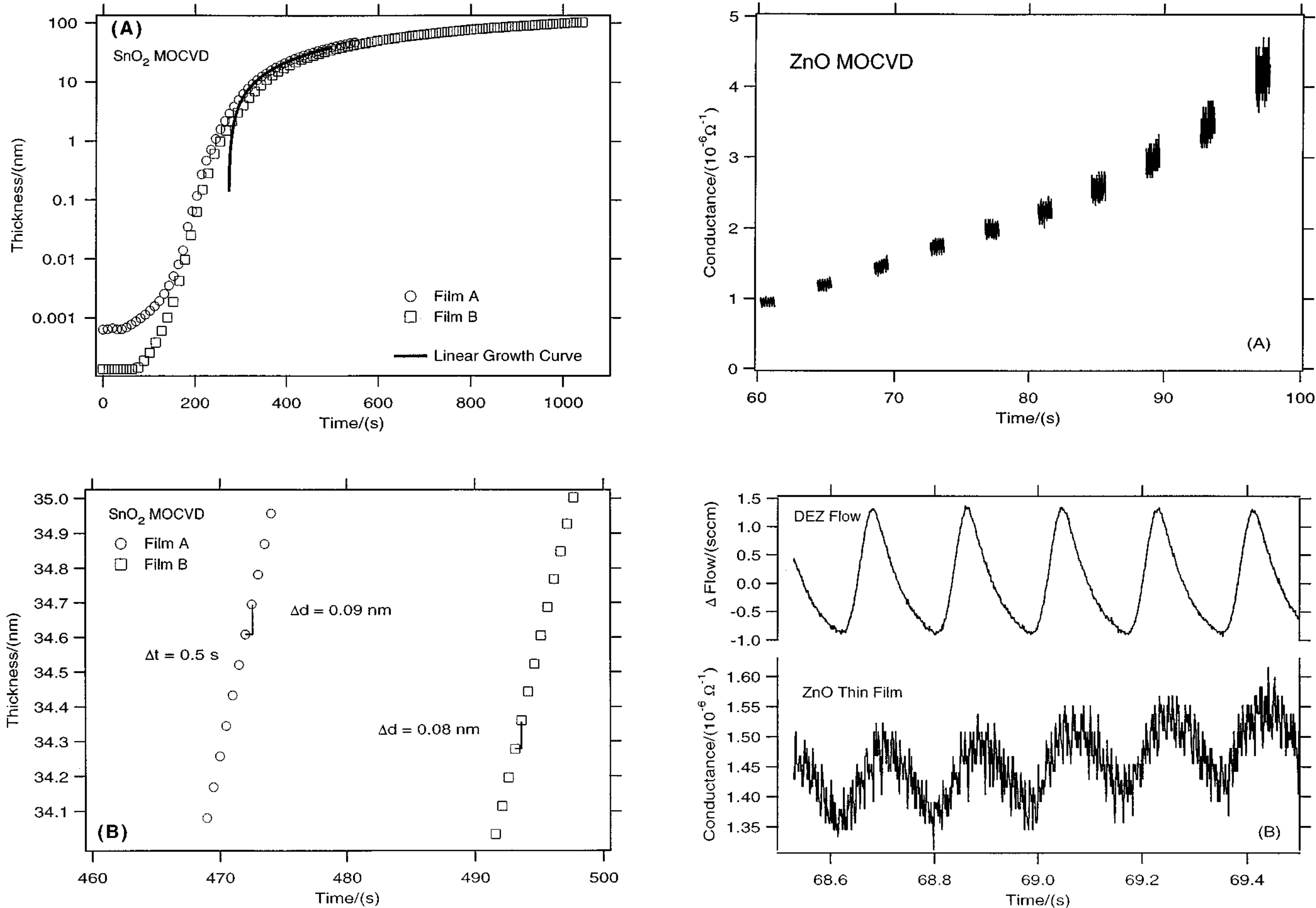

FIG. 8. (A) Semilog plot of the thickness vs time data in Fig. 6(A). The solid line is the extrapolation of the linear growth region. (B) Expanded scale plot of the thickness vs time data in Fig. 6(A) indicating an equivalent thickness sensitivity on the order of an angstrom.

FIG. 9. (A) *In situ* conductance vs time data for the growth of a ZnO thin film collected using an oscilloscope. Gaps are due to the periodic transfer of data from the oscilloscope to the computer. (B) The lower panel is an expanded region of ZnO conductance, and the upper panel is the simultaneously acquired error signal taken from the mass flow controller that regulates the flow over the DEZ.

would not have a negative slope at any point. A physical interpretation that is more likely is that the variations in the conductivity are the result of surface interactions that are a function of the DEZ concentration, e.g., variations in the zinc-precursor/oxygen ratio that is absorbed on the entire film surface. Variations in the DEZ concentration were determined to be due to oscillations in the Ar carrier gas flow due to faulty mass flow controller performance. This is shown by the data in the top panel of Fig. 9(B), which is the output flow of the mass flow controller (as measured by the 0–5 V flow signal) and was measured simultaneously on the same oscilloscope. The variations in the conductance of the ZnO film lag behind the ebb and flow of the carrier gas passing over the precursor by $\sim$2 ms. This is the time it takes the variation in the flow to reach the microhotplate, and is in rough agreement with an estimated transit time of 5 ms. [This velocity estimation was based on the mass flow rate of the carrier gas (80 sccm) at a working pressure of 0.665 Pa, and an approximate straight path length of 1 m through 0.47-cm diameter tubing.] When the oscillations in the precursor gas were removed by stabilizing the mass flow controller, the oscillations in the film conductance also disappeared. The conductance of the growing ZnO film is then comprised of two parts. The first part is the baseline (or average) monotonic increase with increasing film thickness, on top of which is superimposed an oscillation in the film conductance due to surface reactions with the changing DEZ concentration. The film was ''gas sensing'' the atmosphere from which it was growing, and this was subsequently used to identify and correct an otherwise undetectable process variation. Although it appears from Fig. 9(A) that the amplitude of the oscillation is increasing with time, in fact it is the noise level in the measurement, most likely due to a poor contact, that is increasing and not the oscillation amplitude.

IV. CONCLUSIONS

Using silicon-based micromachining techniques, we have developed an *in situ* conductance measurement technique for the study of semiconducting oxide thin films deposited by MOCVD. The competing effects of variations in conductivity and thickness can be deconvoluted from each other through the use of additional characterization techniques.

Downloaded 14 Jan 2013 to 202.38.84.14. Redistribution subject to AVS license or copyright; see http://avspublications.org/jvsta/about/rights_and_permissions

This provides useful insight into the deposition process, and results in improved deposition control. Analysis of the thickness versus time data indicates that this technique has angstrom sensitivity. Finally, *in situ* conductance measurements provide a unique window into the MOCVD process, indicating in one case the malfunction of a mass flow controller that would have otherwise gone undetected. *In situ* conductance measurements are expected to continue to play an important role in our microsensor research.

ACKNOWLEDGMENTS

The authors would like to thank J. Allen, P. Espina, K. Kreider, R. Raman, B. Shomaker, and E. Xu for their valuable assistance. The authors would also like to thank M. Vaudin for his critical review of this article. Two of the authors (F.D. and N.H.T.) gratefully acknowledge the support of the NIST/NRC Postdoctoral Associateship Program.

[1] P. T. Moseley, A. M. Stoneham, and D. E. Williams, in *Techniques and Mechanisms in Gas Sensing*, edited by P. T. Moseley, J. Norris, and D. E. Williams (Hilger, Bristol, 1991), Chap. 4, pp. 108.
[2] N. Taguchi, UK Patent No. 1,280,809 (1970).
[3] F.-C. Lin, Y. Takao, Y. Shimizu, and M. Egashira, Sens. Actuators B **24**, 843 (1995).
[4] J. S. Suehle, R. E. Cavicchi, M. Gaitan, and S. Semancik, IEEE Electron Device Lett. **14**, 118 (1993).
[5] R. E. Cavicchi, J. S. Suehle, K. G. Kreider, B. L. Shomaker, J. A. Small, and M. Gaitan, Appl. Phys. Lett. **66**, 812 (1995).
[6] S. Semancik, R. E. Cavicchi, M. Gaitan, and J. S. Suehle, US Patent No. 5,345,213 (1994).
[7] Commercial products are identified only to specify experimental procedure. This in no way implies recommendation or endorsement by the National Institute of Standards and Technology.
[8] S. Semancik, R. E. Cavicchi, K. G. Kreider, J. S. Suehle, and P. Chaparola, Sens. Actuators B **34**, 209 (1996).
[9] F. DiMeo, Jr., S. Semancik, R. E. Cavicchi, J. S. Suehle, P. Chaparala, and N. H. Tea, Mater. Res. Soc. Symp. Proc. **415**, 231 (1996).
[10] F. DiMeo, Jr., S. Semancik, R. E. Cavicchi, J. S. Suehle, N. H. Tea, and J. T. Kelliher, Mater. Res. Soc. Symp. Proc. **441**, 69 (1997).
[11] F. DiMeo, Jr., S. Semancik, R. E. Cavicchi, J. S. Suehle, N. H. Tea, M. D. Vaudin, and J. T. Kelliher, Mater. Res. Soc. Symp. Proc. **444**, 203 (1997).
[12] J.-L. Pouchou and F. Pichoir, in *Electron Probe Quantitation*, edited by K. F. J. Heinrich and D. E. Newbury (Plenum, New York, 1991), p. 31.

Downloaded 14 Jan 2013 to 202.38.84.14. Redistribution subject to AVS license or copyright; see http://avspublications.org/jvsta/about/rights_and_permissions